Supporting Information:
Heat-transport mechanisms in molecular building blocks of inorganic/organic hybrid superlattices

Ashutosh Giri,[1] Janne-Petteri Niemelä,[2] Tommi Tynell,[2] John T. Gaskins,[1]
Brian F. Donovan,[1] Maarit Karppinen,[2] and Patrick E. Hopkins[1,*]

[1]*Department of Mechanical and Aerospace Engineering, University of Virginia, Charlottesville, Virginia 22904, USA*

[2]*Department of Chemistry, Aalto University, FI-00076 Aalto, Finland*

(Dated: February 19, 2016)

Table S1. Thicknesses for all the samples measured via XRR.

Sample	Thickness (nm)	Density (g cm^{-3})
ALD-grown ZnO	154.0	5.4
$ZnO_{x=13.1\ nm}$/HQ	91.1	-
$ZnO_{x=7.0\ nm}$/HQ	93.3	-
$ZnO_{x=3.9\ nm}$/HQ	97.2	-
$ZnO_{x=1.4\ nm}$/HQ	93.8	3.3
$ZnO_{x=0.7\ nm}$/HQ	82.7	2.4
ALD-grown TiO_2	98.3	3.65
$(TiO_2)_{x=15.5\ nm}$/HQ	92.7	-
$ZnO_{x=0.7\ nm}$/3 HQ	81.2	-
$ZnO_{x=0.7\ nm}$/5 HQ	93.1	-
$ZnO_{x=0.7\ nm}$/7 HQ	90.1	-

EXPERIMENTAL

The film thicknesses and densities measured *via* XRR are shown in Table S1.

Figure S1 shows the measured values for the front side ($h_{\mathrm{K,Al/ZnO}}$) and back side ($h_{\mathrm{K,ZnO/Al_2O_3}}$) conductances in the temperature range of 78-300 K studied in this work. These conductances present a major source of uncertainty in the measured values of thermal conductivities for the $ZnO_{x=7nm}$/HQ and $ZnO_{x=13nm}$/HQ samples. Therefore, to provide further confidence to the independently measured values of these conductances from our control sample (using the in-phase signal), we show three contour plots that demonstrate the deviation of the 3-layer model from the ratio ($-V_{\mathrm{in}}/V_{\mathrm{out}}$) as a function of $h_{\mathrm{K,Al/ZnO}}$ and $h_{\mathrm{K,ZnO/Al_2O_3}}$ with κ_{ZnO} fixed to 42 W m^{-1} K^{-1}, deviation as a function of $h_{\mathrm{K,Al/ZnO}}$ and κ_{ZnO} with $h_{\mathrm{K,ZnO/Al_2O_3}}$ fixed, and finally deviation as a function of κ_{ZnO} and $h_{\mathrm{K,ZnO/Al_2O_3}}$ with $h_{\mathrm{K,Al/ZnO}}$ fixed (Fig. S2). These sensitivity contour plots represent the mean square deviation of the 3-layer model to the ratio of the in-phase and out-of-phase signals with the various combinations of input parameters in the model.[1] As shown in Fig. S2a, with the thermal conductivity of ZnO set to 42 W m^{-1} K^{-1} (as measured for a purely ALD grown ZnO thin film in Ref 2), the front side and back side conductances predicted from our 3-layer model agree with the values measured from V_{in} by fitting the signal for the first

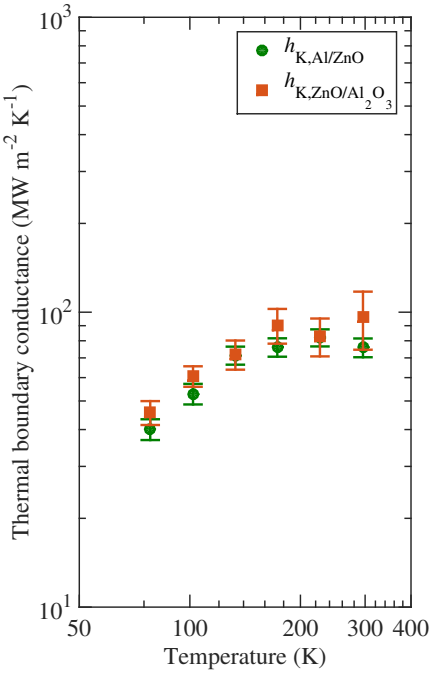

Figure S1. Measured thermal boundary conductances for the Al/ZnO (red squares) and ZnO/Al_2O_3 (green circles) interfaces for the range of temperatures studied in this work.

nanosecond. However, as shown in Fig. S2b and c, a large range of values for κ_{ZnO} can produce the best fit in the least squares sense. Therefore, it is not possible to accurately determine κ_{ZnO} from our analysis of the experimental data. This is due to the fact that the ALD-grown ZnO thin film is very thermally conductive and our analytical model is not sensitive to κ_{ZnO}. Although, we cannot measure κ_{ZnO} accurately, the values for the front side and back side conductances that produce the best-fit of our model to the ratio of the TDTR signals agree with our measurements of these conductances (from V_{in} by fitting at various time delays), thus supporting the use of the measured values of front side and back side conductances as input parameters in the model that is used to measure the thermal conductivities of our hybrid SL films. Note, for the hybrid SLs with high interface densities (x=3.9, 1.4, 0.7 nm), the three-layer model losses sensitivity to the front side and back side conductances, which presents comparatively low uncertainties as the thermal conductivity of the hybrid films decrease.

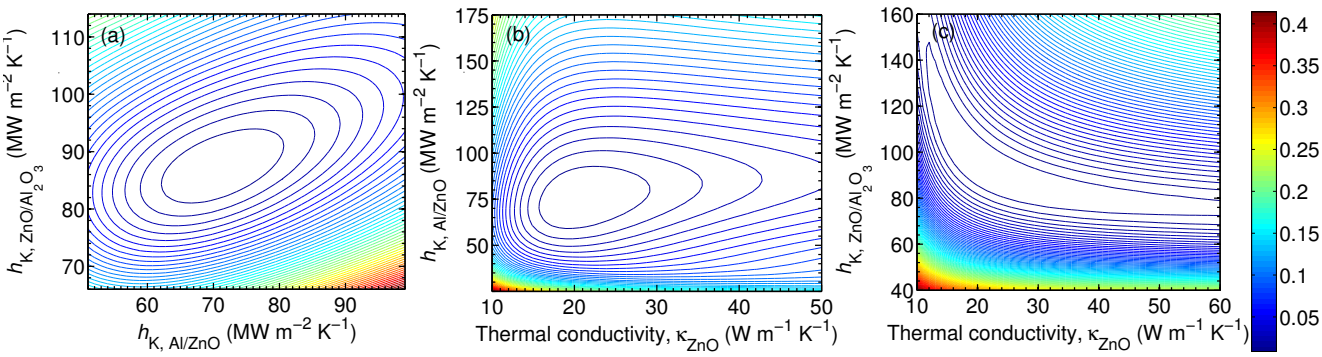

Figure S2. Sensitivity contour plots showing the interrelationship between the various input parameters in the 3-layer thermal model for the purely ALD grown ZnO thin film at 8.8 MHz pump modulation frequency and room temperature.

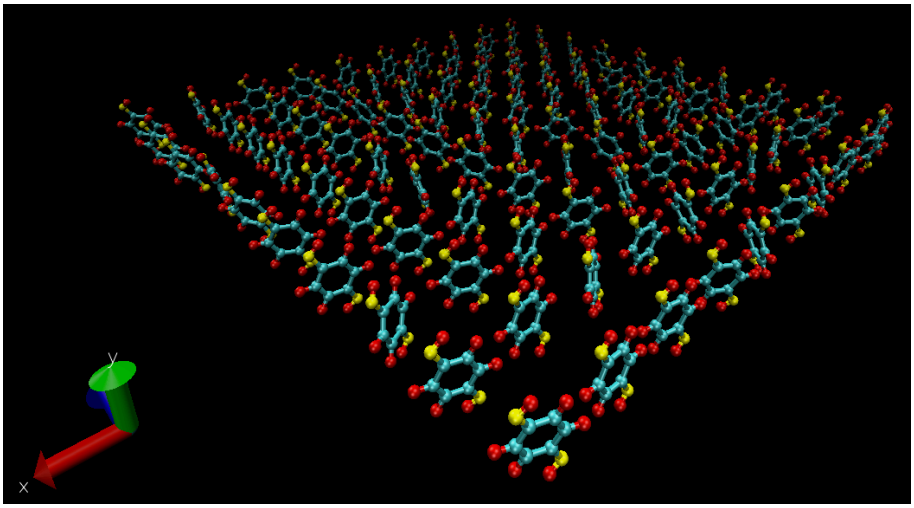

Figure S3. Schematic of the MD computational domain with 1400 atoms representing the HQ monolayer interspersed between the inorganic layers. The green atoms are Carbon, yellow atoms are Oxygen and the red atoms are hydrogen.

MOLECULAR DYNAMICS SIMULATION

We performed molecular dynamics (MD) simulations using the LAMMPS package [4] to compute the local phonon density of states in a monolayer of HQ molecules. The schematic of the MD domain containing 1400 atoms is shown in Fig. S3. We use the ReaxFF interatomic potential to describe the interactions between the atoms in the HQ molecules [5]. We use periodic

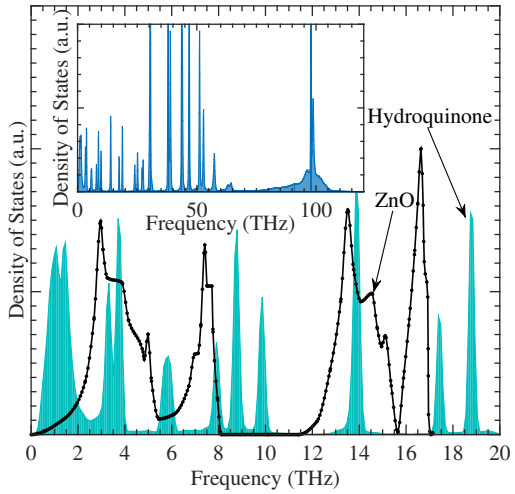

Figure S4. Comparison of vibrational density of states for a HQ layer (obtained via molecular dynamics) and ZnO (obtained from phonon dispersion in Ref. 3). (inset) The complete local phonon density of states for the HQ layer showing the discrete spikes at a range of phonon frequencies.

boundary conditions in the x-and z-directions and use the shrink-wrap boundary condition on the y-direction. The top and bottom oxygen and hydrogen atoms in the y-direction are held fixed so as to replicate the conditions in a monolayer of MLD-grown HQ molecules constrained in between the inorganic layers. The computational domain was first equilibrated at a predefined temperature of 300 K under the Nose-Hoover thermostat [6] for a total of 3×10^5 time steps using a time step of 0.25 fs. After equilibration, the velocities of the unconstrained atoms were recorded every 10 time steps for a total of 1×10^5 time steps using a NVE scheme to create a velocity fluctuation time series [7]. The density of states, $D(\omega)$, is obtained from the Fourier Transform ($\mathcal{F}$) of the velocity autocorrelation function (*VACF*).[8] The Welch method of power spectral density estimation is applied to obtain the $D(\omega)$ and is normalized as follows,

$$D(\omega) = \frac{1}{2} m \mathcal{F}(VACF) \frac{1}{k_{\mathrm{B}} T} \rho \tag{1}$$

where m is the atomic mass, k_{B} is the Boltzmann constant, T is the local temperature, and ρ is the atomic density.

Figure S4 compares the local phonon density of states of the simulated HQ layer to the phonon spectra of ZnO calculated from the phonon dispersion in Ref. 3). As shown, the density of states do not overlap completely and therefore the phonon transport can not be described by the DMM that predicts a maximum phonon transmission of 50% at an ideal interface. The inset of Fig. S4

shows the full spectral density of states for the HQ layer calculated by the procedure described above.

THEORETICAL CALCULATIONS

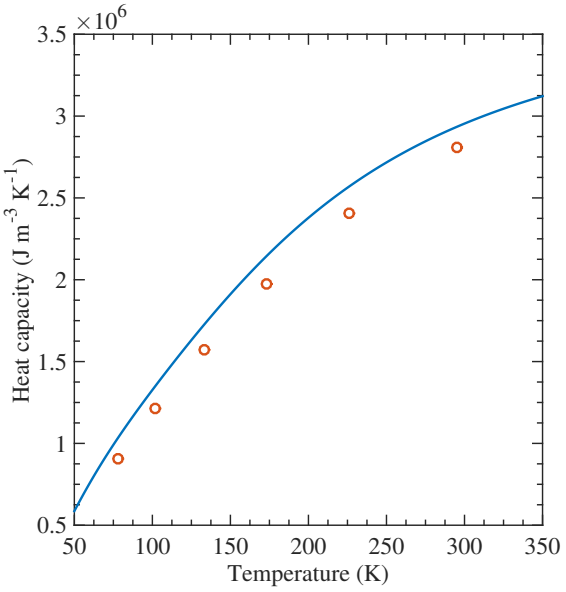

Figure S5. Comparison of the experimentally measured heat capacity in Ref. 9 (hollow circles) to the values predicted by Eq. 3 (solid line).

To gain insight into the experimental results, we consider the phonon flux in the inorganic layer. In the most general form, the heat flux in a crystal approaching an interface is given by,

$$q = \frac{1}{8\pi^3} \sum_j \int_{k_x} \int_{k_y} \int_{k_z} \hbar\omega f v_{g,j} \cos\theta dk_x dk_y dk_z, \tag{2}$$

where ω is the phonon angular frequency, k is the wave-vector, f is the phonon distribution, $v_{g,j}\cos\theta$ is the phonon group velocity in the direction of the applied thermal gradient and j is the phonon polarization. To simplify the calculations, we assume a spherical symmetry to the hexagonal Brillouin Zone for ZnO and use the phonon dispersion relation in the $\Gamma \rightarrow \mathrm{M}$ direction as given in Ref. 3. By considering the dispersion in only one direction, we assume that the phononic flux is isotropic and that the phonon dispersion in the $\Gamma \rightarrow \mathrm{M}$ direction can fully capture the heat transport (along the 100 direction in the ZnO layers) analyzed in our experiments. For our calculations,

we fit 3rd order and 4th order polynomials to the phonon dispersion (from Ref. 3) and estimate the wave vector at the edge of the Brillouin Zone as $\pi/V^{\frac{1}{3}}$, where V is the calculated equilibrium volume at zero pressure (as calculated from *ab initio* calculations in Ref. 3). To validate these assumptions, we use the phonon dispersion to calculate the heat capacity, C_{V}, of ZnO as,

$$C_{\mathrm{V}} = \sum_{j} \int_{0}^{\omega_{c,j}} \hbar\omega D_j(\omega) \frac{\partial f}{\partial T} \mathrm{d}\omega \tag{3}$$

Figure S5 compares the predicted C_{V} from our calculations using the fitted phonon dispersion to the experimentally measured C_{V} for ZnO in Ref. 9. Our calculations agree well with the experimentally measured values, validating our assumptions.

To calculate the phonon flux for TiO_2, we use the phonon dispersion relation in the $\Gamma \rightarrow \mathrm{X}$ direction as given in Ref. 10. Using full polynomials to capture the realistic phonon dispersion in this direction while assuming an isotropic Brillouin Zone in TiO_2 overpredicts the heat capacity of the material by an order of magnitude, which is mainly due to the anisotropy in the crystal structure of TiO_2. Therefore, we only consider the first three branches (i.e., the 2 transverse acoustic and the 1 longitudinal acoustic branches) and fit 3rd order and 4th order polynomials to the phonon dispersion. Calculation of Eq. 3 by considering these three branches predicts a reasonably agreeable value of heat capacity at room temperature (C_{V}=2.9$\times$10^6 J m^{-3} K^{-1}) compared to the bulk value determined from density functional theory (C_{V}=2.7$\times$10^6 J m^{-3} K^{-1}) [10]. We estimate the wave vector at the edge of the Brillouin Zone as $2\pi/a$, where a=3.79 Å [10] is the lattice parameter.

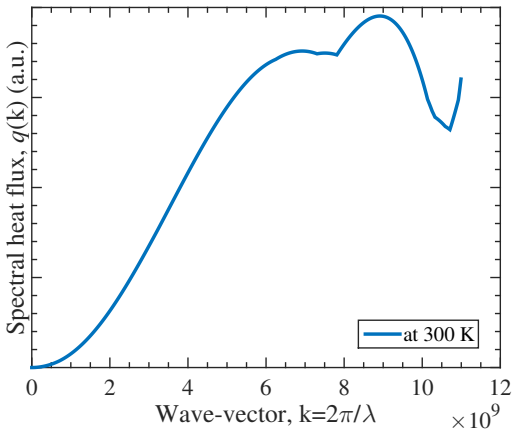

Figure S6. Spectral heat flux in ZnO as a function of the wave-vector in the $\Gamma \rightarrow \mathrm{M}$ direction.

In order to study the role of the vibrational properties of the organic layers contributing to the less than unity transmission coefficient, we calculate the spectral heat flux in the ZnO layer as a function of the wave-vector of phonons in the $\Gamma \rightarrow \mathrm{M}$ direction (Fig. S6). The spectral heat flux provides quantitative measurements of the percent heat flux carried by different wavelength phonons. The length of the hydroquinone molecules used as the organic constituent are $\sim$6-7 Å and therefore, we hypothesize that phonons with wavelengths greater than the length of the organic molecule chain are unaffected by the vibrational properties of the molecules, whereas those with wavelengths less than the length of the molecule chains are scattered similar to the analogy of photons in an absorptive media (Beer- Lambert law). Our calculations demonstrate that $\sim$9-25% of the heat flux is carried by phonons with wavelengths shorter than the length of the organic molecules ($\sim$6-7 Å). This result is consistent with the high transmission coefficients (average values of $\sim$76% for the $(\mathrm{ZnO})_{7.0}$ nm/HQ sample and $\sim$65% for the $(\mathrm{ZnO})_{13.1}$ nm/HQ sample for the 78-300 K temperature range) measured from our TDTR measurements. Note, the transmission did not show any significant temperature dependency under the experimental uncertainty in our results.

Similarly, for the TiO_2-based SL, we determine a transmission of $\sim$41%, a value much lower than that for the ZnO based SLs. The spectral heat flux calculations for TiO_2 demonstrates that the percent heat flux carried by phonons with wavelengths shorter than $\sim$6-7 Å in TiO_2 is $\sim$53-62%, which agrees reasonably well with the $\sim$41% transmission determined from the experiment. This result strengthens our argument that phonons with wavelengths longer than the molecular lengths used for the organic layers in the SL are less affected by the vibrational properties of the molecules than the shorter wavelength phonons.

* phopkins@virginia.edu

[1] J. P. Feser and D. G. Cahill, Review of Scientific Instruments **83**, 104901 (2012).

[2] J. Alvarez-Quintana, E. Martínez, E. Pérez-Tijerina, S. A. Pérez-García, and J. Rodríguez-Viejo, Journal of Applied Physics **107**, 063713 (2010).

[3] J. Serrano, F. Manjón, A. Romero, A. Ivanov, M. Cardona, R. Lauck, A. Bosak, and M. Krisch, Phys. Rev. B **81**, 174304 (2010).

[4] S. Plimpton, Journal of Computational Physics **117**, 1 (1995).

[5] A. Strachan, A. C. T. van Duin, D. Chakraborty, S. Dasgupta, and W. A. Goddard, Phys. Rev. Lett. **91**, 098301 (2003).

[6] W. G. Hoover, Phys. Rev. A **31**, 1695 (1985).

[7] J. C. Duda, T. S. English, E. S. Piekos, W. A. Soffa, L. V. Zhigilei, and P. E. Hopkins, Phys. Rev. B **84**, 193301 (2011).

[8] M. P. Allen and D. J. Tildesley, *Computer Simulation of Liquids (Oxford Science Publications)*, reprint ed., Oxford science publications (Oxford University Press, 1989).

[9] C. Klingshirn, A. Waag, A. Hoffmann, and J. Geurts, *Zinc Oxide: From Fundamental Properties Towards Novel Applications*, Vol. 120 (Springer, 2010).

[10] Z.-G. Mei, Y. Wang, S.-L. Shang, and Z.-K. Liu, Inorganic Chemistry **50**, 6996 (2011).